energies

MDPI

Article

The Influence of Protective Coatings on High-Temperature Corrosion under Biomass Ash Deposits

Anna Maciejczyk [1,2], Izabella Maj [3,*], Szymon Ciukaj [4], Bartłomiej Hernik [3] and Arkadiusz Osuch [1]

[1] SHI FW Energia Fakop Sp. z o.o., 41-200 Sosnowiec, Poland; anna.maciejczyk@shi-g.com (A.M.); arkadiusz.osuch@shi-g.com (A.O.)
[2] Doctoral School, Silesian University of Technology, 44-100 Gliwice, Poland
[3] Department of Power Engineering and Turbomachinery, Faculty of Energy and Environmental Engineering, Silesian University of Technology, 44-100 Gliwice, Poland; bartlomiej.hernik@polsl.pl
[4] Sumitomo SHI FW Energia Polska Sp. z o.o., 41-200 Sosnowiec, Poland; szymon.ciukaj@shi-g.com
* Correspondence: izabella.maj@polsl.pl

Abstract: The presented research determined the performance of the protective coatings against the corrosion process under biomass and refuse-derived fuel (RDF) ash deposits. High-temperature corrosion tests were performed on steel grades intended for use in the fabrication of pressure parts working in elevated temperatures such as superheaters in power boilers. Two steel grades were investigated, P235GH and 16Mo3, and two protective coatings were applied, Inconel 625 and Alloy 310. The samples were sourced from the industrial boiler manufacturing company. The samples were exposed to two ashes originating from biofuels and one ash originating from RDF for comparison, all collected from Polish heat plants and power plants. Exposures were carried out in an oxidizing atmosphere for a maximum time of 504 h. The test temperatures of 480, 520, and 580 °C simulated superheater conditions of biofuel- and waste-fired power boilers. The corrosion kinetics were determined by weight change measurements conducted after 24, 168, and 504 h of the exposure. Regardless of the exposure temperature and the type of ash under which the samples were investigated, the use of 2.0 mm thick protective coatings resulted in smaller increases in the weight of the tested coupons which proves that alloy coatings give measurable results and are good remedies for chlorine-induced corrosion.

Keywords: biomass; corrosion; combustion; ash; RDF; coating; Inconel 625; Alloy 310

check for updates

Citation: Maciejczyk, A.; Maj, I.; Ciukaj, S.; Hernik, B.; Osuch, A. The Influence of Protective Coatings on High-Temperature Corrosion under Biomass Ash Deposits. *Energies* **2023**, *16*, 7221. https://doi.org/10.3390/en16217221

Academic Editor: Eliseu Monteiro

Received: 14 September 2023
Revised: 17 October 2023
Accepted: 21 October 2023
Published: 24 October 2023

Copyright: © 2023 by the authors. Licensee MDPI, Basel, Switzerland. This article is an open access article distributed under the terms and conditions of the Creative Commons Attribution (CC BY) license (https://creativecommons.org/licenses/by/4.0/).

1. Introduction

High-temperature corrosion, fouling, and slagging of heated surfaces are vital issues in boilers utilizing fuels with high alkali and chlorine contents. Especially, the combustion of biomass [1–4], as well as waste and refuse-derived fuel (RDF) [5–9], is reported to cause severe material degradation in heat exchangers. With growing interests in biomass and waste utilization, these problems must be investigated and properly addressed. Nevertheless, studying the corrosion process in industrial boilers is difficult due to its unstable nature, usually causing full-scale research to be challenging or even impossible. Therefore, the literature provides some lab-scale corrosion experiments conducted under different atmospheric conditions and temperature ranges using various steel grades.

These experiments can be broadly categorized into two main types: corrosion research involving metal samples under chlorine- and alkali-consisting deposits [10–22], and research focusing on metal sample corrosion in a chlorine-rich atmosphere [23–26]. In the case of chlorine- and alkali-consisting deposit tests, researchers mainly used pure chlorine or potassium compounds like KCl, $PbCl_2$, K_2SO_4, or their mixtures. Steel coupons are usually covered with salt deposits, placed in a heated chamber for varying durations ranging from 48 h [21] up to over 600 h [20] and exposed to temperatures between 320 °C [22] and 950 °C [18]. The corrosion process is typically investigated using methods such as weight

change measurement and, in most research, the weight change in mg/cm^2 is recorded. The temperature and the presence of alkalis and chlorine were found to have the most significant impact on the corrosion rate. For instance, Metsäjoki et al. [19] studied uncoated and slurry aluminized 9–12 wt% Cr steels under KCl deposits at temperatures of 560 °C and 610 °C. After 336 h of exposure, the weight gain was reported to exceed 11 mg/cm^2 when KCl was present in the deposit and HCl was present in the atmosphere. Zhang et al. [12] investigated superheated steel samples under KCl deposits in the temperature range of 450–650 °C where the increase in temperature significantly affected the corrosion kinetics with the corrosion rate at 650 °C being reported to be 16 times higher than that at 450 °C.

The corrosiveness of pure ash deposits has been less extensively studied compared to synthetic salts and their mixtures. The few available studies [27–32] mainly focus on biomass ash in its pure form and enriched with alkaline salts to enhance the corrosion potential. For instance, Mlonka-Medrala et al. [29] investigated several boiler steel types, including 16Mo3, 10Cr9-10, X10CrMoVNb9–1, and X7CrNiNb18–10, under biomass ash deposits doped with 0.1% and 0.5% KCl. After an exposure time of 168 h, the highest mass gain of 8.7 mg/cm^2 was reported for the 10CrMo9-10 sample under ash deposit doped with 0.5% of KCl at 610 °C, whereas almost no mass gain was observed for X7CrNiNb18–10 and pure ash. In a similar study by Bankiewicz et al. [32], the influence of pure oat and rye straw on the corrosion of 10CrMo9-10 at 550 °C and 600 °C was investigated and found to be negligible which could be attributed to the low chlorine content of the straw. The research presented in [31] includes the comparison of high- and low-chlorine biomass types, namely cow manure and mixed straw, whose corrosion influence on 16Mo3 and 10Cr9-10 steel grades was investigated in the temperature range of 460–560 °C. In the case of high-chlorine cattle manure ashes, a mass gain of above 6 mg/cm^2 was reported in the highest investigated temperature with an exposure time of 168 h.

Most of the research listed above deals with common boiler steel grades. Boiler steel for the power industry is known as alloy steel and carbon steel, intended for use where the operating temperature is high, usually >600 °C. The main task of steel grades used for boiler construction is primarily to prevent and shorten the progression time of deformation and fatigue of a particular boiler part that is exposed to high operating temperatures, corrosive environments, and loads. The proper steel grade selection is a result of several factors like whether the material of a given grade has an optimal thermal resistance to hot flue gases, appropriate weldability, ductility, as well as relaxation and corrosion resistance. As the power boiler is a pressure part during operation, the most important parameters of boiler steel are the creep limit, creep strength, the yield point at a specific temperature, and heat resistance. The boiler steel grade investigation regarding the impact of thermal loads on pressure and non-pressure parts in power boilers is presented in [33].

Implementing protective coatings is an efficient remedy for the corrosive wear of boiler tubes and can significantly prolong the working span of heat exchangers. The coatings are usually made of nickel-based alloys and applied by different technologies such as welding, cladding, or thermal spraying. Czupryński et al. [34] investigated the performance of thermally sprayed coatings exposed to a hydrogen chloride-containing atmosphere for up to 1000 h and a temperature of 800 °C. The coatings made of Ni-Cr-B-Si alloy demonstrated a 50% higher resistance to high-temperature corrosion in comparison to coatings made of Ni-B-Si alloy. Both coatings showed indisputably lower susceptibility to corrosion than non-coated low-alloy steel commonly used for heat exchangers. Hruska et al. [35] investigated thermally sprayed Ni-based coatings in up to 5000 h of exposure at 500 and 600 °C in a model HCl-containing atmosphere. The specimens with coatings did not show signs of corrosion. Most of the coatings tested showed comparable or higher corrosion resistance than the highly alloyed austenitic steel AISI 310 and were significantly more corrosion-resistant than the 16Mo3 steel commonly used for the manufacturing of heat exchangers in power boilers. The above studies present the investigation of protective

coatings exposed to an HCl-containing atmosphere while the challenge of predicting the effectiveness of coatings under ash deposits remains poorly understood.

The presented research aims to determine the performance of the protective coatings against high-temperature corrosion under pure biomass and RDF ash deposits in oxidizing conditions. The most widely used boiler steel grades, P235GH and 16Mo3, were investigated. The steels were protected with two welded coatings of 2.0 mm thickness: Inconel 625 and Alloy 310. The temperature range of 480–580 °C was applied, which corresponds to the standard temperature of heat-exchanging surfaces in biomass and waste-fired boilers. Two biomass types and one RDF type, all originating from Polish units, were investigated. According to the Authors' best knowledge and the research cited above, little attention has been given to the investigation of the high-temperature corrosion involving pure ash deposits and even less when it comes to research involving protective coatings. This highlights a significant knowledge gap and therefore, the present study represents a novel and unique research endeavor. The results can enhance the interest in biomass energy conversion.

2. Materials and Methods

2.1. Steel Grades and Coatings

The tested steel grades are commonly utilized in boiler construction, particularly in the construction of superheaters and waterwalls, which are susceptible to chlorine-induced corrosion. These steels exhibit different chromium contents and varying expected levels of corrosion resistance. The composition analysis of the steel samples provided by the manufacturers (16Mo3 and P235GH) and the protective coatings (Inconel 625 and Alloy 310) are detailed in Table 1.

Table 1. Elemental compositions of investigated steel grades and coatings (wt%).

Element	16Mo3	P235GH	Inconel 625	Alloy 310
C	0.12—0.2	max. 0.16	0.03–0.1	0.08–0.15
Si	max. 0.35	max. 0.35	max. 0.5	max. 0.65
Mn	0.4–0.9	0.6–1.2	max. 0.5	01.02.2005
Ni	max. 0.3	max. 0.3	min 58	20–22.5
P	max. 0.025	max. 0.025	max. 0.02	max. 0.03
S	max. 0.01	max. 0.015	max. 0.015	max. 0.03
Cr	max. 0.3	max. 0.3	20–23	25–28
Mo	0.25–0.35	max. 0.08	8–10	max. 0.75
N	max. 0.012	max. 0.012	-	-
Cu	max. 0.3	max. 0.3	max. 0.5	max. 0.75
Nb	-	max. 0.02	-	-
Ti	-	max. 0.03	max. 0.4	-
Al.	-	max. 0.02	max. 0.4	-
V	-	max. 0.02	-	-
Fe	-	-	max. 5	-
Co	-	-	max. 1	-
Cr + Cu + Mo + Ni	-	<0.7	-	-

Both P235GH and 16Mo3 are the most widely used boiler steel grades. The P235GH is a non-alloy steel and 16Mo3 is a molybdenum steel alloy commonly used for the construction of a wide range of pressure vessels, especially in elevated working temperatures, boilers, and heat exchangers. The steels were protected with two welded coatings of 2.0 mm thickness: Inconel 625 and Alloy 310.

Inconel 625 belongs to the group of austenitic nickel-based alloys. Due to its high resistance to corrosion, erosion, and oxidation, Inconel 625 performs well in demanding and extreme environments that are exposed to high pressure and temperature. It creates a thick, stable passivating oxide layer, which is an effective barrier to the corrosion processes.

Additionally, this coating maintains strength over a wide temperature range, which is particularly important in high-temperature operation conditions. A detailed study on Inconel 625 weld overlaying methods for P235GH and 16Mo3 steel is presented in [36]. Alloy 310 is also austenitic stainless steel developed for use in highly corrosive operation conditions. It has a high chromium content and a moderate nickel content so it can effectively protect steel against corrosion processes.

2.2. Fuel Characteristics

Two types of biomasses and one refuse-derived fuel were considered in this study. The samples were collected from Polish combustion units where they were utilized in power boilers for the production of heat and electricity. The following samples are investigated:

P1—Wood biomass collected from a power plant located in south-east Poland. The biomass is utilized in a circulating fluidized bed (CFB) boiler.

P2—Refuse-derived fuels (RDF) collected from a power unit in southern Poland.

P3—Wood biomass collected from a heat and power plant in southern Poland. The biomass is utilized in a circulating fluidized bed (CFB) boiler.

The selected characteristics of the fuels were determined and are given in Table 2. The following parameters were determined according to the European standards for biomass (P1 and P3) and waste-derived fuels (P2): ash content by weight method according to PN-EN ISO 18122:2016-01 [37] and PN-EN ISO 21656:2021-08 [38], moisture content by weight method according to PN-EN ISO 18134-2:2017-03 [39] and CEN/TS 154-2:2010 [40], Lower Calorific Value (LHV) and Higher Calorific Value (HHV) by calorimetry according to PN-EN ISO 18125:2017-07 [41] and PN-EN ISO 21654:2021-12 [42], the contents of C, H and N by Infrared (IR) analyzer according to PN-EN ISO 16948:2015-07 [43] and PN-EN ISO 21663:2021-06 [44], S contents according to PN_EN ISO 16994:2016-10 [45] and PN-EN 15408:2011 [46], and Cl contents by the Ion Chromatography (IC) method according to PN-EN ISO 16994:2016-10 [45] and PN-EN 15408:2011 [46].

Table 2. Proximate and elemental (ultimate) analyses of fuel samples.

Sample	Moisture	Ash	HHV	LHV	C	H	N	S	Cl
	%	%	MJ/kg	MJ/kg	%	%	%	%	%
P1	42.6	2.1	19.84	18.55	50.5	5.91	0.31	0.04	0.013
P2	15.4	33.85	19.33	18.3	44.59	5.56	1.28	0.35	0.56
P3	59.1	12.3	18.98	17.75	47.86	5.66	0.54	0.05	0.033

2.3. Ash Preparation and Characteristics

The fuel samples were placed into a ceramic crucible, heated up to 550 °C, and incinerated in a constant temperature zone in an electric muffle furnace. As a result, chemically stable ash with a minimal amount of unburned carbon (UBC) was obtained for further analyses. The oxide ash composition and ash fusion temperatures (AFT) are presented in Tables 3 and 4. These parameters were determined since they are the most common procedures for ash characterization in terms of corrosion risk and other combustion-related issues. The ash composition was determined by Inductively Coupled Plasma-Optical Emission Spectroscopy (ICP-OES). The ash fusion temperatures were determined by the microscope-photographic method according to standard CEN/TS 15404:2010 [47]. The procedure covers the identification and recording of shrinkage starting temperature (SST), deformation temperature (DT), hemisphere temperature (HT), and flow temperature (FT). The specific characteristic shapes of the ash cylinders were recorded by a digital system. The procedure took place at a maximum temperature of 1500 °C.

Table 3. Ash compositions (dry basis, wt%).

Sample	SiO_2	Fe_2O_3	Al_2O_3	Mn_3O_4	TiO_2	CaO	MgO	SO_3	P_2O_5	Na_2O	K_2O	BaO	SrO
P1	54.50	1.60	3.97	1.11	0.25	16.80	2.64	1.63	1.73	0.49	5.75	0.11	0.05
P2	48.60	3.23	12.8	0.10	1.19	15.10	2.28	1.66	0.72	5.74	1.16	0.21	0.07
P3	72.80	1.49	3.09	0.53	0.25	8,16	1.09	0.81	1.50	0.50	4.00	0.05	0.02

Table 4. Ash fusion temperatures.

	P1	P2	P3
Shrinkage Starting Temperature (SST)	1180 ± 60	1040 ± 80	1270 ± 95
Deformation temperature (DT)	1200 ± 60	1070 ± 80	>1500 ± 75
Hemisphere temperature (HT)	1220 ± 65	1190 ± 65	>1500 ± 75
Flow temperature (FT)	1310 ± 70	1200 ± 60	>1500 ± 75

2.4. Corrosion Experiments

Laboratory experiments were conducted to study the corrosion resistance of the investigated coatings throughout 504 h (21 days). The tests took place in the laboratory of SHI FW Energia Fakop Sp. Z o.o. located in Sosnowiec, Poland, in a muffle furnace with a continuous supply of air to maintain the oxidizing atmosphere. The exposition temperatures of 480, 520 and 580 °C were chosen as they reflect the temperature conditions on the surface of heat exchangers in biomass and waste boilers. Mass measurements of samples were taken after 24, 168 and 504 h to determine the corrosion kinetics.

Coupons of each steel grade measuring 25 × 25 mm were prepared by cutting steel tubes, followed by polishing using SiC paper with varying grain sizes from 240 to 1200. These coupons were then cleaned in an ultrasonic bath with acetone to eliminate any contaminants. Figure 1 illustrates the appearance of the prepared steel coupons. Subsequently, the coupons were positioned in ceramic crucibles, with the upper surface covered by the ash, as depicted in Figure 2. The lower surface remained unexposed and was not factored into the calculations. The samples were then subjected to a 504-h exposition in an electrically heated chamber with discontinuous mass measurements taken after 24, 168 and 504 h of exposition.



Figure 1. Steel coupons prepared for corrosion experiments.



Figure 2. Steel coupons covered with ashes.

2.5. Slagging Factors

Numerous indexes have been developed to classify fuels in terms of potential unwanted issues that may take place in the furnace [29,48–51]. These methods enable the prediction of problems such as ash agglomeration, slagging, fouling, or high-temperature corrosion. They primarily rely on the chemical composition of ash, its fusion temperatures, and the characteristics of the fuel, mainly chlorine content. In the presented research, the 15 indexes were gathered and applied to the investigated fuels to assess their tendencies to slagging, fouling, and high-temperature corrosion. Table 5 lists these indexes, along with their evaluations, indicating whether the fuel poses a low, moderate, high, or extremely high risk.

Table 5. Slagging factors and their evaluation criteria [48,52–54].

Factor	Formula	Evaluation
Silica content in the ash	SiO_2 [%]	<20—low 20–25—moderate >25—high
Quotient (SA) of silica oxide and alumina oxide	$SA = \frac{SiO_2}{Al_2O_3}$	<1.87—niskie 1.87–2.65—moderate >2.65 bardzo wysokie
Chlorine content in the fuel	Cl [%] as received	<0.2—low 0.2–0.3—moderate 0.3–0.5—high >0.5—very high
Basic-to-acidic oxide ratio	$\frac{B}{A} = \frac{Fe_2O_3+CaO+MgO+Na_2O+K_2O}{SiO_2+Al_2O_3+TiO_2}$	<0.5—low 0.5–1.0—moderate 1.0–1.75—high >1.75—very high
Basic-to-acidic oxide ratio + potassium	$\frac{B}{A} + P = \frac{Fe_2O_3+CaO+MgO+Na_2O+K_2O+P_2O_5}{SiO_2+Al_2O_3+TiO_2}$	<0.5—low 0.5–1.0—moderate 1.0–1.75—high >1.75—very high
Basic-to-acidic oxide ratio simplified	$B/A_{simplified} = \frac{Fe_2O_3+CaO+MgO}{SiO_2+Al_2O_3}$	<0.5—low 0.5–1.0—moderate 1.0–1.75—high >1.75—very high

Table 5. *Cont.*

Factor	Formula	Evaluation
Babcock Index	$Rs = \frac{B}{A} * S^d$ where: S^d—sulfur content in dry fuel	<0.6—low 0.6–2.0—moderate 2.0–2.6—high >2.6—very high
Fouling factor	$Fu = \frac{B}{A} * (Na_2O + K_2O)$	<0.6—low 0.6–40.0—moderate >40.0—high
Quotient of sulfur and chlorine	2S/Cl	>4—low <1—high
Sintering Indicator	$SI = \frac{CaO+MgO+Na_2O+K_2O+Fe_2O_3+P_2O_5}{SiO_2+Al_2O_3+TiO_2}$	<0.75 and >2.0—low 0.75–2.0—high and very high
Bed Agglomeration Index	$BAI = \frac{Fe_2O_3}{Na_2O+K_2O}$	>0.15—low <0.15 high
Ash Fusibility Index	$AFI = \frac{4*IT+HT}{5}$ where: IT—Initial Deformation Temperature; HT—Hemisphere temperature	>1342—low 1232–1342—moderate 1052–1232—high <1052—very high
Iron to Calcium ratio	$IC = \frac{Fe_2O_3}{CaO}$	<0.3 and >3.0—low 0.3–3.0—high
Slag Viscosity Index	$S_R = SiO_2 * \frac{100}{SiO_2+Fe_2O_3+CaO+MgO}$	>72—low 65–72—moderate <65—high
Initial Deformation Temperature	IDT [°C]	>1100—low 900–1100—moderate <900—high

3. Results and Discussion

3.1. Slagging Factors

Table 6 presents the results of 16 indexes applied to the investigated fuels together with their evaluations, indicating whether the fuels pose a low, moderate, high, or extremely high risk of slagging.

Table 6. Slagging factor results.

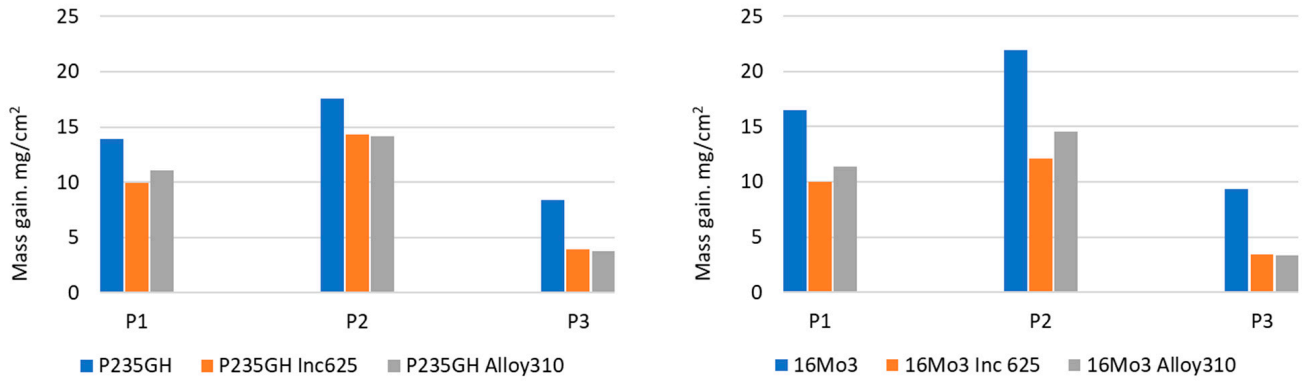
Factor	Symbol	P1		P2		P3	
		Result	Evaluation	Result	Evaluation	Result	Evaluation
Silica content in the ash	SiO_2 [%]	54.3	high	48.6	high	72.8	high
Quotient (SA) of silica oxide and alumina oxide	SA	13.68	very high	3.80	very high	23.56	very high
Chlorine content in the fuel	Cl [%]	0.013	low	0.56	very high	0.033	low
Basic-to-acidic oxide ratio	B/A	0.466	low	0.44	low	0.20	low
Basic-to-acidic oxide ratio + potassium	(B/A) + P	0.496	low	0.451	low	0.22	low
Basic-to-acidic oxide ratio simplified	$B/A_{simplified}$	0.361	low	0.336	low	0.141	low
Babcock Index	Rs	0.019	low	0.154	low	0.01	low
Fouling index Fu	Fu	2.909	moderate	3.033	moderate	0.90	moderate
Quotient of sulfur and chlorine	2S/Cl	6.154	low	1.25	moderate	3.03	moderate
Sintering Indicator	SI	0.496	low	0.451	low	0.220	low
Bed Agglomeration Index	BAI	0.256	low	0.468	low	0.331	low
Ash Fusibility Index	Fs	6020	low	5470	low	7500	low
Iron to Calcium ratio	IC	0.095	low	0214	low	0.183	low
Slag Viscosity Index	S_R	72.073	low	70.221	moderate	87.154	low
Initial Deformation Temperature	IDT [°C]	1200	low	1070	moderate	1500	low

Initially, these indexes were established for coal ashes, but researchers are now exploring their suitability for biomass ashes. Garcia-Maraver et al. [48] evaluated over a hundred different biomass types using 10 commonly used slagging indexes. The results varied widely with the same fuel being classified as having a low, medium, high, or extremely high slagging risk, depending on the specific factor used. Similarly, the research by Lachman et al. [51] provides an overview of slagging and fouling indicators and their relevance to biomass fuels with various results. Fuels P1 and P3 were categorized as highly or very highly risky by two factors, while fuel P2 by three factors. The main difference is chlorine content which in P2 exceeds 0.5%, while in P1 and P3 is equal to 0.013 and 0.033%, respectively. Therefore, it can be concluded that Cl content may be a crucial factor in the assessment of corrosive potential as suggested in previous research [55,56]

3.2. Corrosion Tests

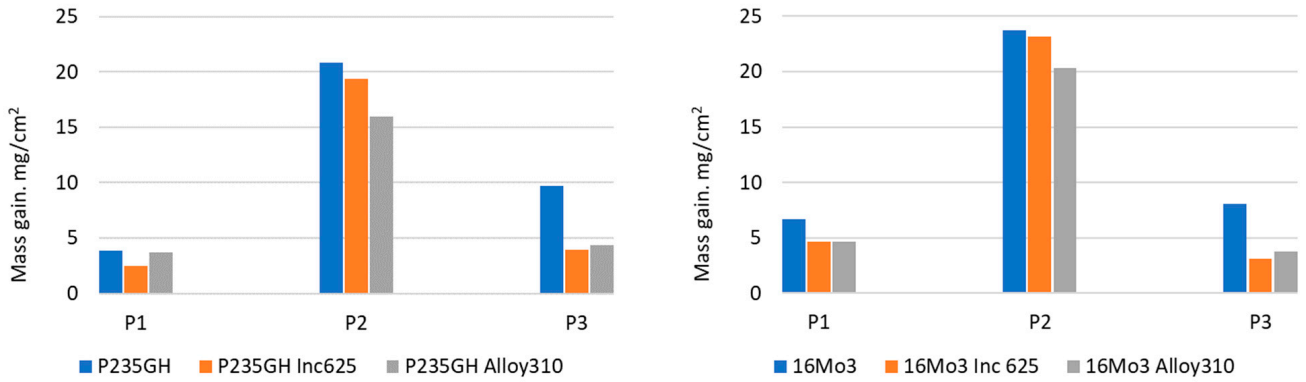
The mass gain of the specimens exposed to the temperatures of 480, 520 and 580 °C after 504 h of exposure are displayed in Figures 3–5, respectively.

The results of corrosion kinetics determined by discontinuous mass change measurements after 24, 168 and 504 h of exposure are displayed in Figure 6a–f for 480 °C, Figure 7a–f for 520 °C and Figure 8a–f for 580 °C.



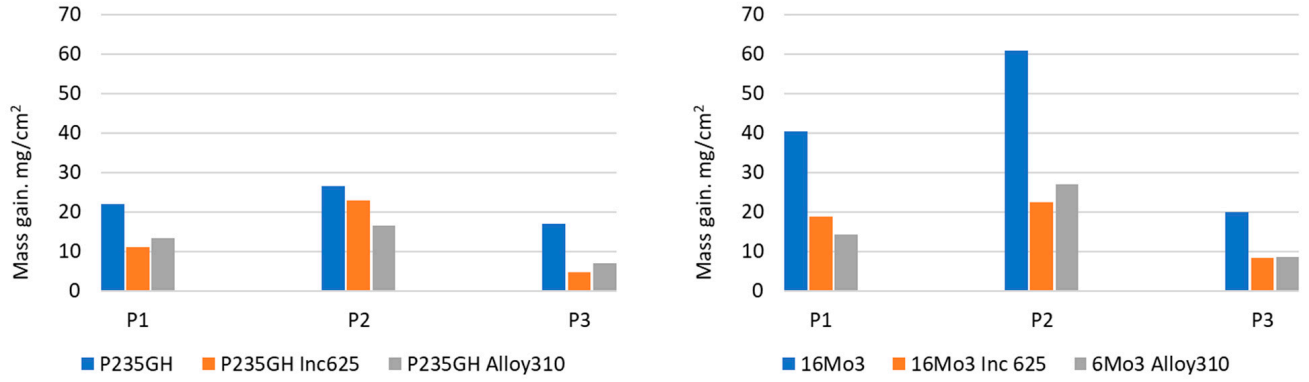
(**a**) (**b**)

Figure 3. Mass gain after 504 h of exposition at 480 °C for P235GH (**a**) and 16Mo3 (**b**).



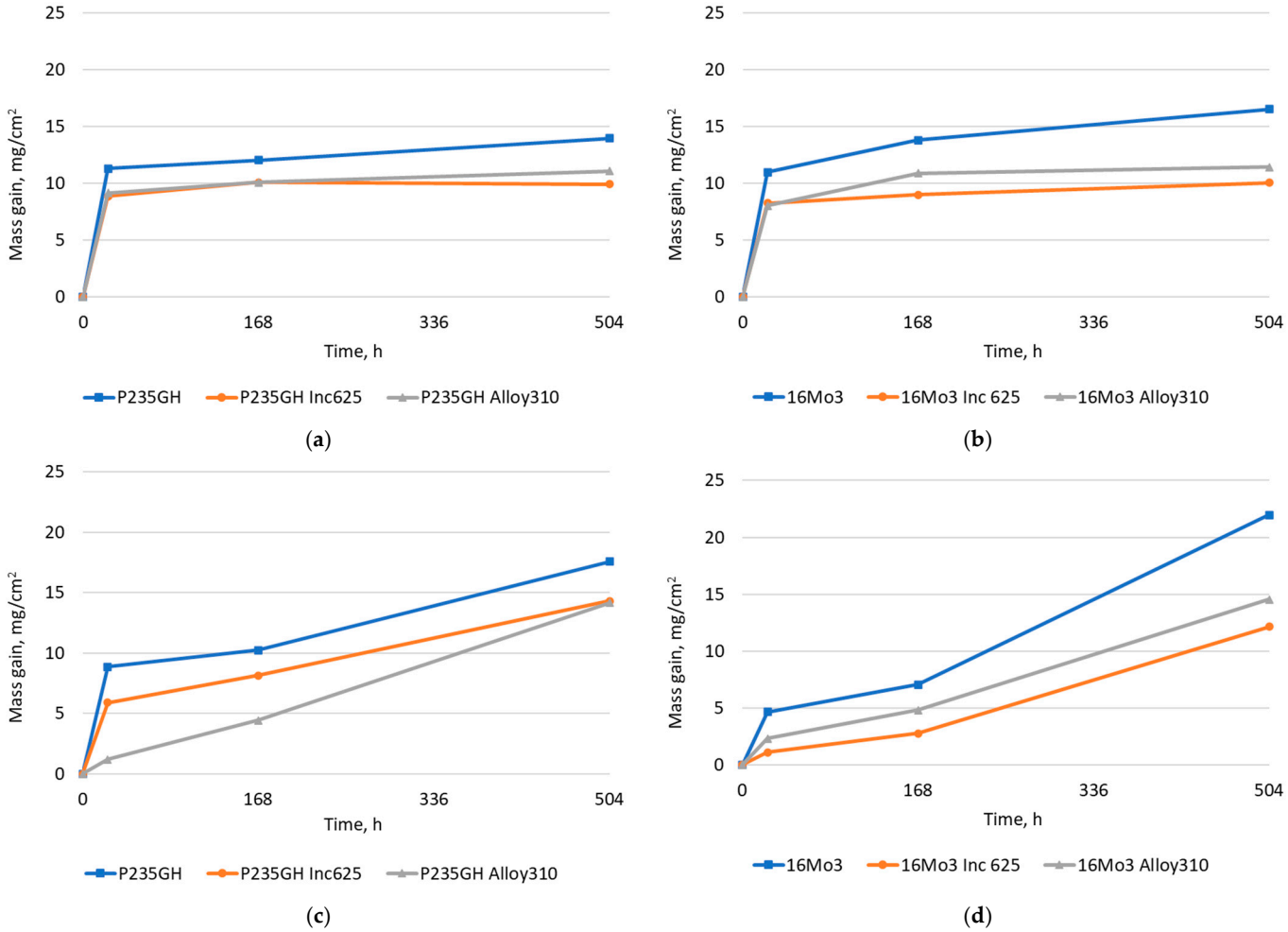
(**a**) (**b**)

Figure 4. Mass gain after 504 h of exposition at 520 °C for P235GH (**a**) and 16Mo3 (**b**).



(**a**) (**b**)

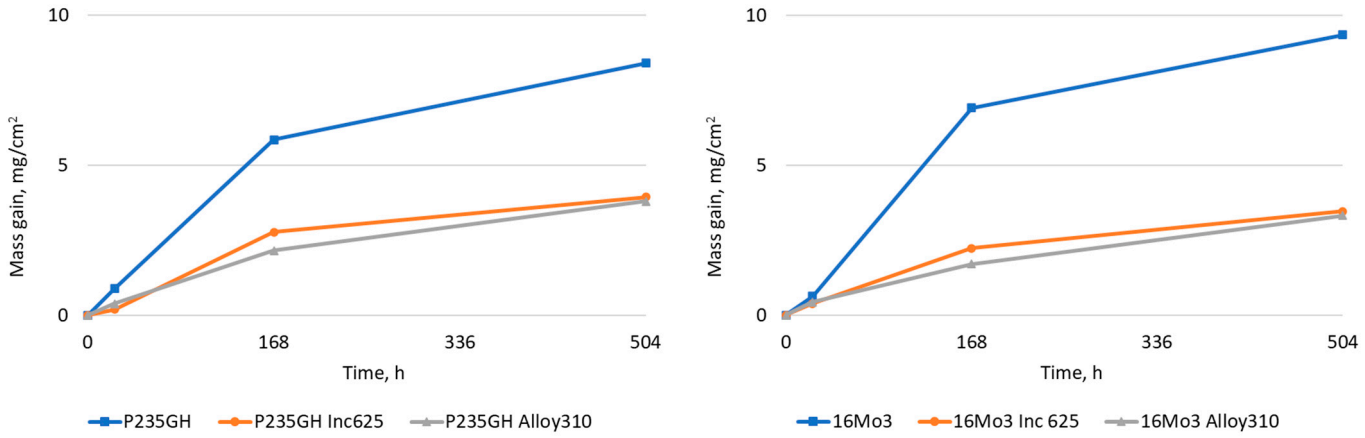
Figure 5. Mass gain after 504 h of exposition at 580 °C for P235GH (**a**) and 16Mo3 (**b**).



(**a**) (**b**)

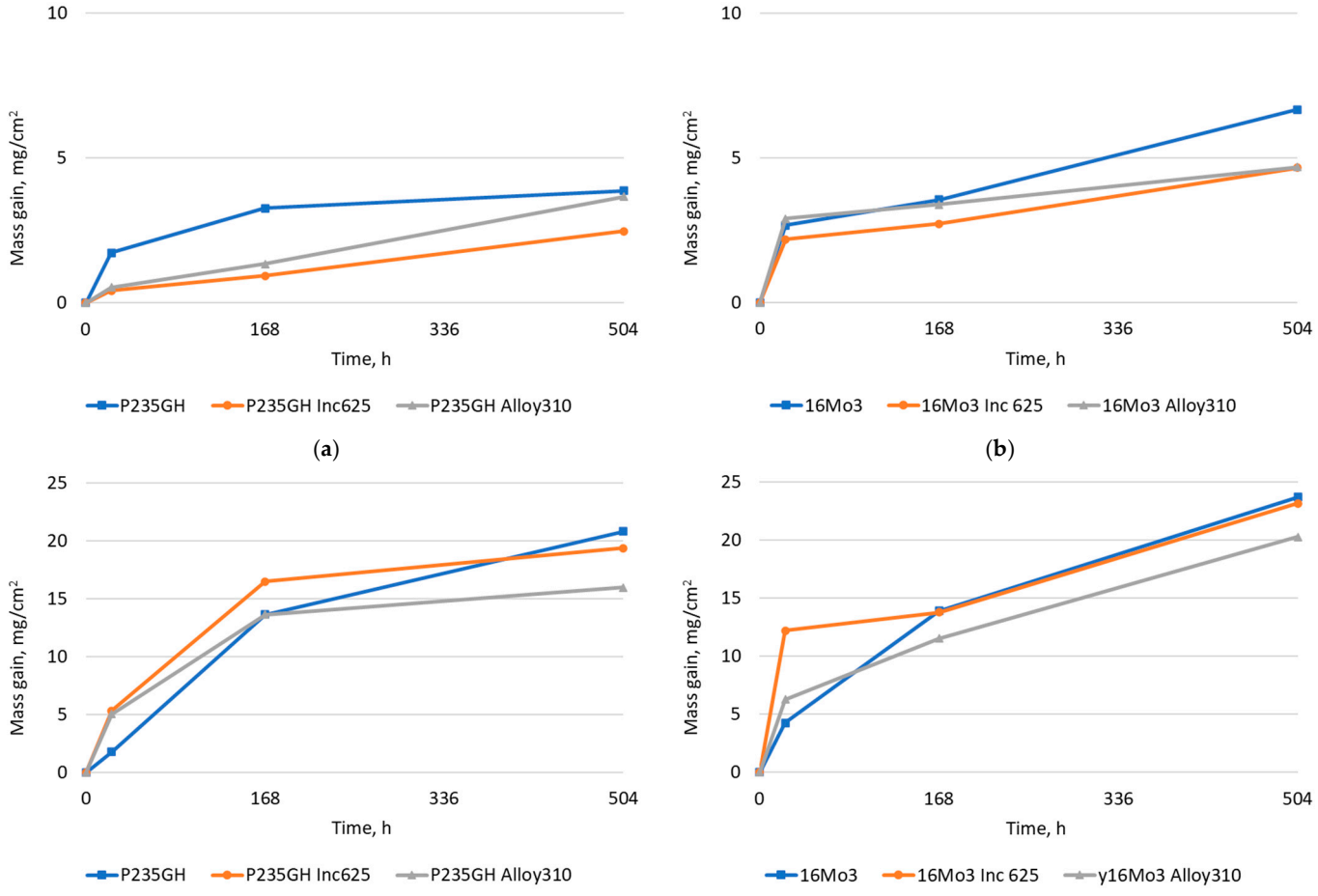
(**c**) (**d**)

Figure 6. *Cont.*



(**e**) (**f**)

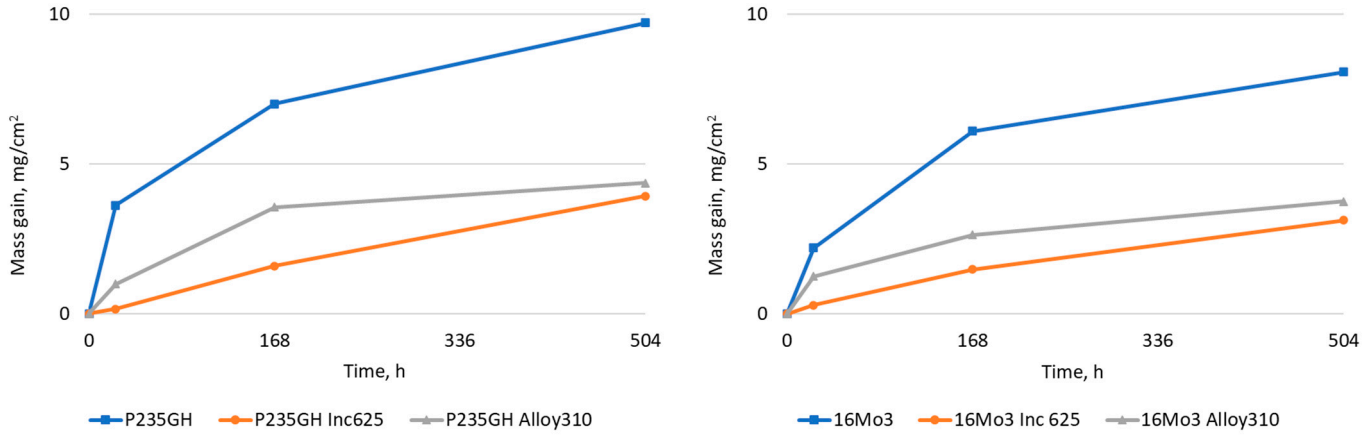
Figure 6. Corrosion kinetics at 480 °C for P235GH under P1 deposits (**a**), 16Mo3 under P1 deposits (**b**), P235GH under P2 deposits (**c**), 16Mo3 under P2 deposits (**d**), P235GH under P3 deposil(**e**), and 16Mo3 under P3 deposits (**f**).



(**a**) (**b**)

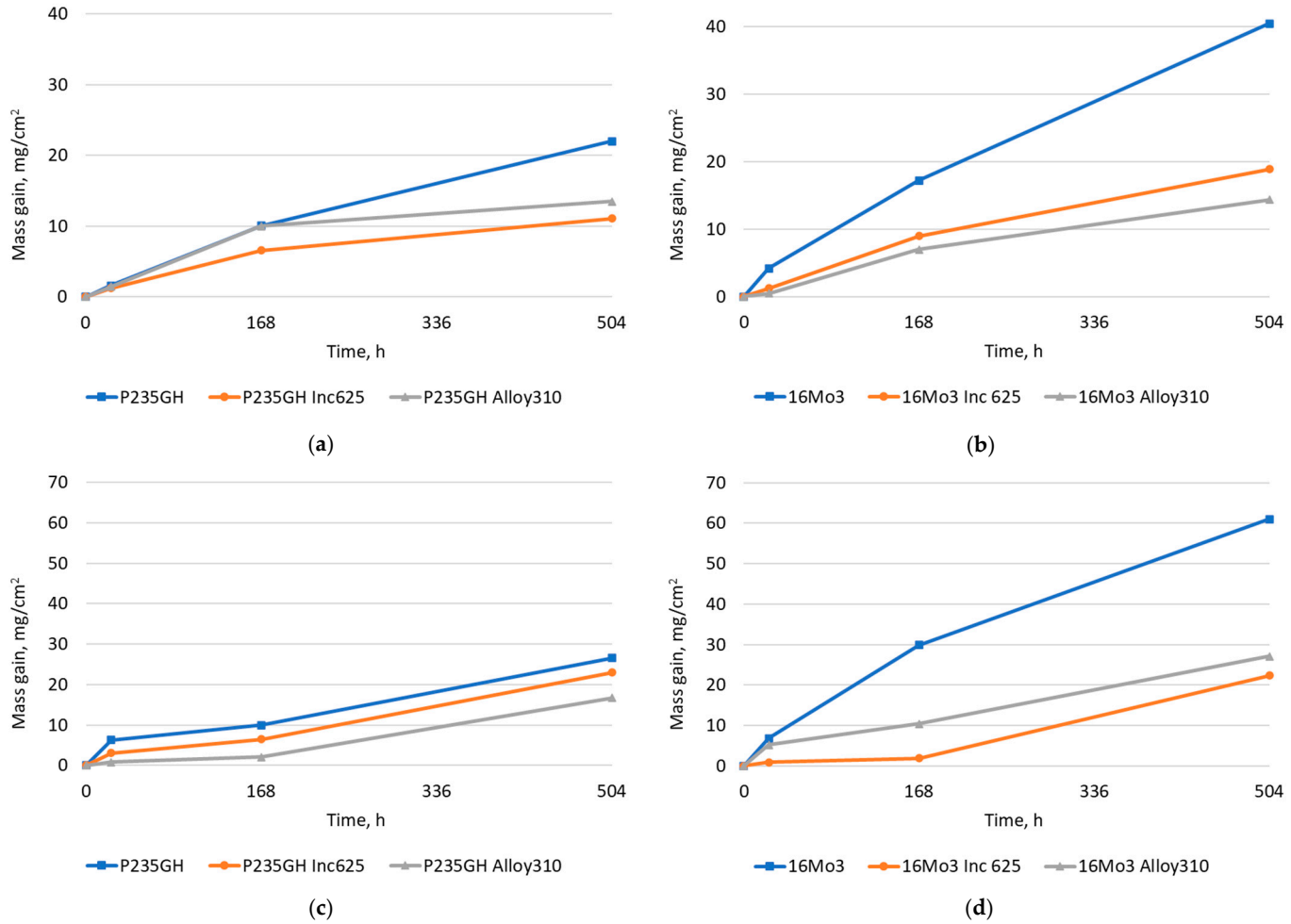
(**c**) (**d**)

Figure 7. *Cont.*



(**e**) (**f**)

Figure 7. Corrosion kinetics at 520 °C for P235GH under P1 depists (**a**), 16Mo3 under P1 depists (**b**), P235GH under P2 depists (**c**), 16Mo3 under P2 depists (**d**), P235GH under P3 deIts (**e**) and 16Mo3 under P3 depists (**f**).



(**a**) (**b**)

(**c**) (**d**)

Figure 8. *Cont.*

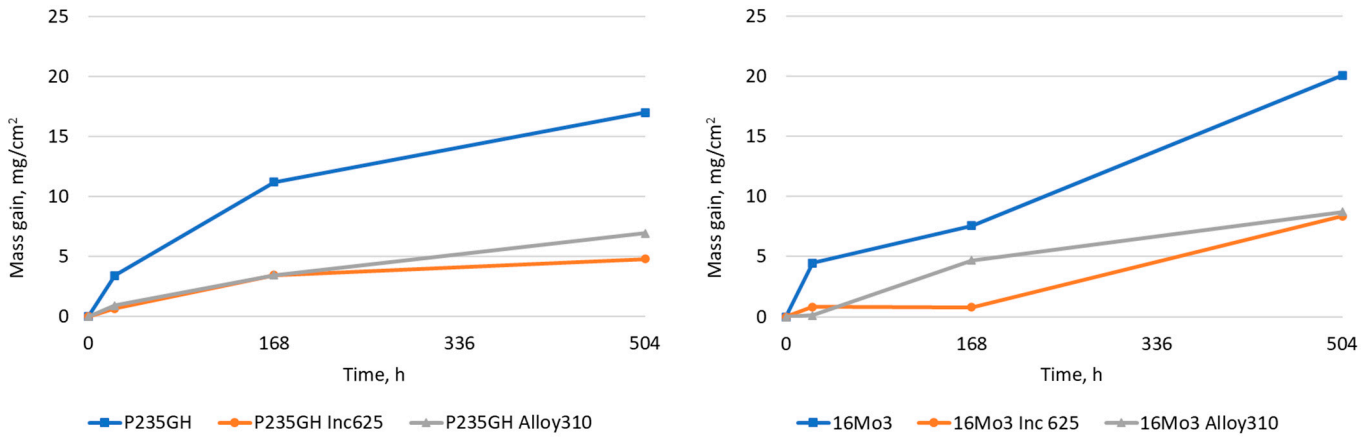


Figure 8. Corrosion kinetics at 580 °C for P235GH under P1 depists (**a**), 16Mo3 under P1 depists (**b**), P235GH under P2 depists (**c**), 16Mo3 under P2 depists (**d**), P235GH unI P3 depists (**e**) and 16Mo3 under P3 depists (**f**).

After 504 h in the furnace at 480 °C, the highest weight gain of 21.96 mg/cm^2 was observed for the 16Mo3 steel coupon without any coating under the P2 ash deposit, as presented in Figure 3a,b. All 16Mo3 coupons with welded coatings revealed visibly smaller weight increases, i.e., protecting the steel with Inconel 625 material resulted in a reduction in the corrosion rate by approximately 45% and with Alloy310 material by approximately 33%. A similar tendency was seen for P1 and P3 ash deposits. Nevertheless, the lower chlorine concentration in P1 and P3 fuel samples caused the corrosion to be less intense, reaching 16.50 and 9.34 mg/cm^2, respectively, for uncoated 16Mo3 samples. In the case of P1 and P3 deposits, the influence of coatings can also be clearly seen, reducing the weight gain. Similarly, for P235GH steel at a temperature of 480 °C, the highest weight gain (17.58 mg/cm^2) was observed under the P2 deposit for the coupon not protected with any coating. In the case of coupons with welding coatings, they showed weight increases that were about 20% lower compared to the uncovered steel coupon, and protection with Inconel 625 material was comparable to the use of Alloy 310 material. As presented in Figure 6a,f, the weight gains of all samples were higher for unprotected coupons in every measuring point after 24, 168 and 504 h.

In the case of an exposure temperature of 520 °C, similar to a temperature of 480 °C, the highest weight increases were observed for coupons not protected with coatings, reaching 20.81 mg/cm^2 for P235 steel and 23.72 mg/cm^2 for 16Mo3 steel, both under P2 deposits, as presented in Figure 4a,b. When the Inconel 625 coating was used, the weight gain slowed down slightly. The difference between the results under P1, P2 and P3 deposits became more intense due to the temperature increase. The corrosive influence of high-chlorine RDF ash deposit (P2) was intensified, which is likely to be the result of the active oxidation mechanism induced by the temperature rise [26,57,58]. For the 16Mo3 under P1 deposits and both steels under P1 deposits, the corrosion process was ambiguous while for other samples the mass gains of unprotected samples were higher in every measurement point (after 24, 168 and 504 h), as can be seen in Figure 7a–f.

According to Figure 5a,b, at a temperature of 580 °C for 16Mo3 steel, the highest weight gain (i.e., 60.99 mg/cm^2) was observed for steel not covered with anti-corrosion protection under P2 ash deposit. This is analogous to the temperature of 480 °C and 520 °C, however, looking directly at the weight gain values, for the temperature of 580 °C they are up to three times higher than when the reference coupons were subjected to a temperature of 480 °C. For the coupons with protective coatings, the weight gains are significantly lower with no specific coating showing a better performance than the other. For the P235GH steel at a temperature of 580 °C, the highest weight gain (i.e., 26.58 mg/cm^2), as in each previous

case, was observed under the P2 deposit for the sample that was not additionally protected against corrosion. When using the Inconel 625 overlay layer, it was visible that the weight gain was twice as small, while the use of Alloy 310 material resulted in a slightly worse reduction in the weight gain. As presented in Figure 8a–f, after 24 h of exposition quite similar weight-increasing tendencies of the samples were observed under P1 deposits for both steel grades and under the P2 deposit for 16Mo3, while after 504 h it was clear that the coating materials provided anti-corrosion protection causing slower mass gains.

The biomass samples P1 and P3 display a relatively low chlorine content of 0.013% and 0.033%, respectively. On the other hand, the RDF sample P2 is characterized by a significantly higher Cl content of 0.56%. The content of chlorine in fuel is crucial, particularly for high-temperature corrosion, as in the combustion chamber it initiates the creation of easily fusible combinations involving metal chlorides. This facilitates the movement of alkali compounds which can combine with silica to form inorganic mixtures, leading to a considerable reduction in the fluid temperature of ash to around 750 °C. Consequently, corrosion induced by chlorine takes place on heat exchanger surfaces following the multi-step active oxidation model, representing the prevailing mechanism of high-temperature corrosion [59].

The higher mass gains in the case of chlorine-rich P2 sample were in line with similar research which indicates severe corrosion damage of steel samples in the presence of chlorine compounds. In the research by Song et al. [60] four coatings were evaluated, and their performance decreased in the presence of KCl deposit which indicated the detrimental effect of chlorine on oxide scales and the acceleration influence of K ions on the chlorine-induced corrosion. For a better understanding of the corrosion process, a scanning electron microscope (SEM) analysis will be conducted as a future research prospect.

As a side work of the presented corrosion rate results, an assessment of the profitability of using each coating was made. After obtaining market data on the purchase cost of Inconel 625 and Alloy 310 wire, and taking into account all other production costs, calculations were made for the cost of making 1 m^2 of the coating welding. Comparing the data obtained and the cost of making a welding with the Alloy 310 material turned out to be 55–60% lower than the cost of making a welding with the Inconel 625 material. Referring this information to the results presented earlier, it can be concluded that it is more profitable to use protective coatings made of Alloy 310 which gives results comparable to Inconel 625 and is more than twice as cheap.

In the case of ash-coated coupons, for the P1 and P3 samples (biomass ashes) at each exposure temperature in the furnace, the results obtained for the Inconel 625 and Alloy 310 coating are very similar, so also in this case the Alloy 310 coating is more profitable. In the case of ash obtained from waste fuel P2 for the P235GH material, a better result in slowing down the corrosion kinetics were achieved for the Alloy 310 coating, while in the case of 16Mo3 steel, Alloy 310 and Inconel 625 coatings after an exposure time of 504 h gave similar results (±8%) with the tendency that Inconel 625 is a better corrosion protection. However, with such a small difference in the weight increase of the tested coupons, it can also be concluded in this case that the use of Alloy 310 coating is a more profitable solution. Therefore, the Alloy 310 coating is currently being implemented in commercial manufacturing by SHI FW Energia Fakop Sp. z o.o.

4. Conclusions

In this research, the effect of 2.0 mm thickness laser coatings Inconel 625 and Alloy 310 on the corrosion resistance of two boiler steel grades was explored. The experiments were conducted under biomass and RDF ash deposits with various characteristics and chlorine contents for exposure times of up to 504 h and temperatures of 480–580 °C.

Analyzing the presented results, it can be noticed that regardless of the exposure temperature of the coupons in corrosive conditions, and regardless of the type of ash with which the samples were investigated, the use of protective coatings resulted in smaller increases in the weight of the tested coupons which proves that alloy coatings give measur-

able results. The Alloy 310 coating caused a similar slowdown in corrosion kinetics to the Inconel 625 coating with lower estimated manufacturing costs.

The main benefit of using coatings is slowing down the kinetics of corrosion and extending the operation lifetime of the power installation and thus, a reduction in material consumption by limiting the frequency of tube repairs which contributes to saving raw materials and energy, even in the case of high-chlorine fuels, such as refuse-derived fuel or high-chlorine biomass.

Author Contributions: Conceptualization, A.M., S.C., B.H. and I.M.; methodology, A.M., S.C., B.H. and I.M.; validation, A.M., S.C., B.H. and I.M.; formal analysis, A.M., S.C., B.H. and I.M.; investigation, A.M.; resources, A.M., A.O. and S.C.; data curation, A.M., S.C., I.M. and B.H.; writing—original draft preparation, I.M., A.M., S.C. and B.H.; writing—review and editing, I.M., A.M., S.C. and B.H.; visualization, I.M. and A.M.; supervision, B.H., S.C. and A.O.; project administration, B.H., S.C., A.M. and A.O.; funding acquisition, B.H., S.C., A.M. and A.O. All authors have read and agreed to the published version of the manuscript.

Funding: This research received no external funding.

Data Availability Statement: The data are available from the corresponding author (I.M.) on request.

Conflicts of Interest: The authors declare no conflict of interest. The funders had no role in the design of the study; in the collection, analyses, or interpretation of data; in the writing of the manuscript; or in the decision to publish the results.

References

1. Sandberg, J.; Karlsson, C.; Fdhila, R.B. A 7year Long Measurement Period Investigating the Correlation of Corrosion, Deposit and Fuel in a Biomass Fired Circulated Fluidized Bed Boiler. *Appl. Energy* **2011**, *88*, 99–110. [CrossRef]
2. Niu, Y.; Tan, H.; Hui, S. Ash-Related Issues during Biomass Combustion: Alkali-Induced Slagging, Silicate Melt-Induced Slagging (Ash Fusion), Agglomeration, Corrosion, Ash Utilization, and Related Countermeasures. *Prog. Energy Combust. Sci.* **2016**, *52*, 1–61. [CrossRef]
3. Król, D.; Motyl, P.; Poskrobko, S. Chlorine Corrosion in a Low-Power Boiler Fired with Agricultural Biomass. *Energies* **2022**, *15*, 382. [CrossRef]
4. Ovčačíková, H.; Velička, M.; Vlček, J.; Topinková, M.; Klárová, M.; Burda, J. Corrosive Effect of Wood Ash Produced by Biomass Combustion on Refractory Materials in a Binary Al–Si System. *Materials* **2022**, *15*, 5796. [CrossRef]
5. Lee, S.-H.; Themelis, N.J.; Castaldi, M.J. High-Temperature Corrosion in Waste-to-Energy Boilers. *J. Therm. Spray Technol.* **2007**, *16*, 104–110. [CrossRef]
6. Persson, K.; Broström, M.; Carlsson, J.; Nordin, A.; Backman, R. High Temperature Corrosion in a 65 MW Waste to Energy Plant. *Fuel Process. Technol.* **2007**, *88*, 1178–1182. [CrossRef]
7. Ma, W.; Wenga, T.; Frandsen, F.J.; Yan, B.; Chen, G. The Fate of Chlorine during MSW Incineration: Vaporization, Transformation, Deposition, Corrosion and Remedies. *Prog. Energy Combust. Sci.* **2020**, *76*, 100789. [CrossRef]
8. Phongphiphat, A.; Ryu, C.; Yang, Y.B.; Finney, K.N.; Leyland, A.; Sharifi, V.N.; Swithenbank, J. Investigation into High-Temperature Corrosion in a Large-Scale Municipal Waste-to-Energy Plant. *Corros. Sci.* **2010**, *52*, 3861–3874. [CrossRef]
9. Verbinnen, B.; De Greef, J.; Van Caneghem, J. Theory and Practice of Corrosion Related to Ashes and Deposits in a WtE Boiler. *Waste Manag.* **2018**, *73*, 307–312. [CrossRef] [PubMed]
10. Meißner, T.M.; Montero, X.; Fähsing, D.; Galetz, M.C. Cr Diffusion Coatings on a Ferritic-Martensitic Steel for Corrosion Protection in KCl-Rich Biomass Co-Firing Environments. *Corros. Sci.* **2020**, *164*, 108343. [CrossRef]
11. Abu-warda, N.; López, A.J.; Pedraza, F.; Utrilla, M.V. Fireside Corrosion on T24 Steel Pipes and HVOF NiCr Coatings Exposed to Different Salt Mixtures. *Corros. Sci.* **2020**, *173*, 108747. [CrossRef]
12. Zhang, J.; ur Rahman, Z.; Wang, X.; Wang, Z.; Li, P.; Wang, Y.; Bate, D.; Zhao, K.; Tan, H. Hot Corrosion Behaviors of TP347H and HR3C Stainless Steel with KCl Deposit in Oxy-Biomass Combustion. *J. Environ. Manag.* **2020**, *263*, 110411. [CrossRef] [PubMed]
13. Yu, X.; Song, P.; He, X.; Khan, A.; Huang, T.; Li, C.; Li, Q.; Lü, K.; Chen, K.; Lu, J. Influence of the Combined-Effect of NaCl and Na2SO4 on the Hot Corrosion Behaviour of Aluminide Coating on Ni-Based Alloys. *J. Alloys Compd.* **2019**, *790*, 228–239. [CrossRef]
14. Vuelvas-Rayo, S.; Gonzalez-Rodriguez, J.G.; Porcayo-Calderon, J.; Salinas-Bravo, V.M.; Maldonado-Ruiz, S.I. Hot Corrosion Behavior of High-Chromium, High-Carbon Cast Irons in NaCl-KCl Molten Salts. *Int. J. Corros.* **2012**, *2012*, 479761. [CrossRef]
15. Kiamehr, S.; Dahl, K.V.; Montgomery, M.; Somers, M.A.J. KCl-Induced High Temperature Corrosion of Selected Commercial Alloys. *Mater. Corros.* **2016**, *67*, 26–38. [CrossRef]
16. Okoro, S.C.; Montgomery, M.; Frandsen, F.J.; Pantleon, K. Time and Temperature Effects on Alkali Chloride Induced High Temperature Corrosion of Superheaters during Biomass Firing. *Energy Fuels* **2018**, *32*, 7991–7999. [CrossRef]

17. Okoro, S.C.; Montgomery, M.; Frandsen, F.J.; Pantleon, K. High Temperature Corrosion under Laboratory Conditions Simulating Biomass-Firing: A Comprehensive Characterization of Corrosion Products. *Energy Fuels* **2014**, *28*, 6447–6458. [CrossRef]
18. Mahajan, S.; Chhibber, R. Hot Corrosion Studies of Boiler Steels Exposed to Different Molten Salt Mixtures at 950 °C. *Eng. Fail. Anal.* **2019**, *99*, 210–224. [CrossRef]
19. Metsäjoki, J.; Huttunen-Saarivirta, E.; Lepistö, T. Elevated-Temperature Corrosion of Uncoated and Aluminized 9–12% Cr Boiler Steels beneath KCl Deposit. *Fuel* **2014**, *133*, 173–181. [CrossRef]
20. Agüero, A.; Baráibar, I.; Gutiérrez, M.; Hernández, M.; Muelas, R.; Rodríguez, S. Biomass Corrosion Behavior of Steels and Coatings in Contact with KCl/K_2SO_4 at 550 °C under an Oxy-Fuel Combustion Atmosphere: A Screening Laboratory Test. *Surf. Coat. Technol.* **2018**, *350*, 188–200. [CrossRef]
21. Pooja, M.; Ravishankar, K.S.; Madav, V. High Temperature Corrosion Behaviour of Stainless Steels and Inconel 625 in Hydroxide Salt. *Mater. Today Proc.* **2021**, *46*, 2612–2615. [CrossRef]
22. Ruh, A.; Spiegel, M. Thermodynamic and Kinetic Consideration on the Corrosion of Fe, Ni and Cr beneath a Molten KCl–ZnCl2 Mixture. *Corros. Sci.* **2006**, *48*, 679–695. [CrossRef]
23. Li, Y.S.; Niu, Y.; Spiegel, M. High Temperature Interaction of Al/Si-Modified Fe–Cr Alloys with KCl. *Corros. Sci.* **2007**, *49*, 1799–1815. [CrossRef]
24. Ma, H.T.; Zhou, C.H.; Wang, L. High Temperature Corrosion of Pure Fe, Cr and Fe–Cr Binary Alloys in O2 Containing Trace KCl Vapour at 750 °C. *Corros. Sci.* **2009**, *51*, 1861–1867. [CrossRef]
25. Jonsson, T.; Folkeson, N.; Halvarsson, M.; Svensson, J.-E.; Johansson, L.-G. Microstructural Investigation of the HCl-Induced Corrosion of the Austenitic Alloy 310S (52Fe26Cr19Ni) at 500 °C. *Oxid. Met.* **2014**, *81*, 575–596. [CrossRef]
26. Alcántara-Cárdenas, J.A.; Ramirez-Lopez, A.; Chávez-Alcalá, J.F.; Sanchez-Pastén, M. Evaluation of High Temperature Corrosion in Simulated Waste Incinerator Environments. *Oxid. Met.* **2016**, *85*, 611–627. [CrossRef]
27. Liu, Y.; Fan, W.; Wu, X.; Zhang, X. Chlorine-Induced High-Temperature Corrosion of Boiler Steels Combusting Sha Erhu Coal Compared to Biomass. *Energy Fuels* **2018**, *32*, 4237–4247. [CrossRef]
28. Mlonka-Mędrala, A.; Gołombek, K.; Buk, P.; Cieślik, E.; Nowak, W. The Influence of KCl on Biomass Ash Melting Behaviour and High-Temperature Corrosion of Low-Alloy Steel. *Energy* **2019**, *188*, 116062. [CrossRef]
29. Mlonka-Mędrala, A.; Magdziarz, A.; Kalemba-Rec, I.; Nowak, W. The Influence of Potassium-Rich Biomass Ashes on Steel Corrosion above 550 °C. *Energy Convers. Manag.* **2019**, *187*, 15–28. [CrossRef]
30. Maj, I.; Kalisz, S.; Wejkowski, R.; Pronobis, M.; Gołombek, K. High-Temperature Corrosion in a Multifuel Circulating Fluidized Bed (CFB) Boiler Co-Firing Refuse Derived Fuel (RDF) and Hard Coal. *Fuel* **2022**, *324*, 124749. [CrossRef]
31. Maj, I.; Kalisz, S.; Szymajda, A.; Łaska, G.; Gołombek, K. The Influence of Cow Dung and Mixed Straw Ashes on Steel Corrosion. *Renew. Energy* **2021**, *177*, 1198–1211. [CrossRef]
32. Bankiewicz, D.; Yrjas, P.; Lindberg, D.; Hupa, M. Determination of the Corrosivity of Pb-Containing Salt Mixtures. *Corros. Sci.* **2013**, *66*, 225–232. [CrossRef]
33. Duda, P.; Felkowski, Ł. Negative Impact of Thermal Loads on Pressure and Non-Pressure Boiler Parts. *Energies* **2023**, *16*, 5768. [CrossRef]
34. Czupryński, A.; Adamiec, J.; Adamiak, M.; Żuk, M.; Kříž, A.; Mele, C.; Kciuk, M. High-Temperature Corrosion of Flame-Sprayed Power Boiler Components with Nickel Alloy Powders. *Materials* **2023**, *16*, 1658. [CrossRef]
35. Hruska, J.; Mlnarik, J.; Cizner, J. High-Temperature Corrosion of Nickel-Based Coatings for Biomass Boilers in Chlorine-Containing Atmosphere. *Coatings* **2022**, *12*, 116. [CrossRef]
36. Rozmus-Górnikowska, M.; Blicharski, M.; Kusiński, J. Influence of Weld Overlaying Methods on Microstructure and Chemical Composition of Inconel 625 Boiler Pipe Coatings. *Kov. Mater.-Met. Mater.* **2014**, *52*, 1–7. [CrossRef]
37. *PN-EN ISO 18122:2016-01*; Solid Biofuels—Determination of Ash Content. Polski Komitet Normalizacyjny: Warszawa, Poland, 2016.
38. *PN-EN ISO 21656:2021-08*; Solid Recovered Fuels—Determination of Ash Content. Polski Komitet Normalizacyjny: Warszawa, Poland, 2021.
39. *PN--EN ISO 18134-2:2017-03*; Solid Biofuels—Determination of Moisture Content. Polski Komitet Normalizacyjny: Warszawa, Poland, 2018.
40. *CEN/TS 154-2:2010*; Paliwa Wtórne—Paliwa Alternatywne: Zawartość Wilgoci Całkowitej. Energopomiar Sp. z o. o.: Gliwice, Poland, 2010.
41. *PN-EN ISO 18125:2017-07*; Solid Biofuels—Determination of Calorific Value. Polski Komitet Normalizacyjny: Warszawa, Poland, 2021.
42. *PN-EN ISO 21654:2021-12*; Solid Recovered Fuels—Determination of Calorific Value. Polski Komitet Normalizacyjny: Warszawa, Poland, 2021.
43. *PN-EN ISO 16948:2015-07*; Solid Biofuels—Determination of Total Content of Carbon, Hydrogen and Nitrogen. Polski Komitet Normalizacyjny: Warszawa, Poland, 2015.
44. *PN-EN ISO 21663:2021-06*; Solid Recovered Fuels—Determination of Total Content of Carbon, hydrogen and nitrogen. Polski Komitet Normalizacyjny: Warszawa, Poland, 2021.
45. *PN_EN ISO 16994:2016-10*; Solid Biofuels—Determination of Total Content of Sulfur and Chlorine. Polski Komitet Normalizacyjny: Warszawa, Poland, 2016.

46. *PN-EN 15408:2011*; Solid Recovered Fuels—Methods for the Determination of Sulphur (S), Chlorine (Cl), Fluorine (F) and Bromine (Br) Content. Polski Komitet Normalizacyjny: Warszawa, Poland, 2011.
47. *CEN/TR 15404:2010*; Paliwa Wtórne—Paliwa Alternatywne: Charakterystyczne Temperatury Topliwości Popiołu. Energopomiar Sp. z o. o.: Gliwice, Poland, 2010.
48. Garcia-Maraver, A.; Mata-Sanchez, J.; Carpio, M.; Perez-Jimenez, J.A. Critical Review of Predictive Coefficients for Biomass Ash Deposition Tendency. *J. Energy Inst.* **2017**, *90*, 214–228. [CrossRef]
49. Weber, R.; Poyraz, Y.; Beckmann, A.M.; Brinker, S. Combustion of Biomass in Jet Flames. *Proc. Combust. Inst.* **2015**, *35*, 2749–2758. [CrossRef]
50. Miles, T.R.; Miles, T.R.; Baxter, L.L.; Bryers, R.W.; Jenkins, B.M.; Oden, L.L. Boiler Deposits from Firing Biomass Fuels. *Biomass Bioenergy* **1996**, *10*, 125–138. [CrossRef]
51. Lachman, J.; Baláš, M.; Lisý, M.; Lisá, H.; Milčák, P.; Elbl, P. An Overview of Slagging and Fouling Indicators and Their Applicability to Biomass Fuels. *Fuel Process. Technol.* **2021**, *217*, 106804. [CrossRef]
52. Jenkins, B.M.; Baxter, L.L.; Miles, T.R.; Miles, T.R. Combustion Properties of Biomass. *Fuel Process. Technol.* **1998**, *54*, 17–46. [CrossRef]
53. Vamvuka, D.; Zografos, D. Predicting the Behaviour of Ash from Agricultural Wastes during Combustion. *Fuel* **2004**, *83*, 2051–2057. [CrossRef]
54. McLennan, A.R.; Bryant, G.W.; Bailey, C.W.; Stanmore, B.R.; Wall, T.F. Index for Iron-Based Slagging for Pulverized Coal Firing in Oxidizing and Reducing Conditions. *Energy Fuels* **2000**, *14*, 349–354. [CrossRef]
55. Maj, I.; Kalisz, S.; Ciukaj, S. Properties of Animal-Origin Ash—A Valuable Material for Circular Economy. *Energies* **2022**, *15*, 1274. [CrossRef]
56. Mlonka-Mędrala, A.; Magdziarz, A.; Gajek, M.; Nowińska, K.; Nowak, W. Alkali Metals Association in Biomass and Their Impact on Ash Melting Behaviour. *Fuel* **2020**, *261*, 116421. [CrossRef]
57. Balint, R.; Engblom, M.; Niemi, J.; Silva da Costa, D.; Lindberg, D.; Yrjas, P.; Hupa, L.; Hupa, M. Temperature Gradient Induced Changes within Superheater Ash Deposits High in Chlorine. *Energy* **2021**, *226*, 120439. [CrossRef]
58. Zahs, A.; Spiegel, M.; Grabke, H.J. Chloridation and Oxidation of Iron, Chromium, Nickel and Their Alloys in Chloridizing and Oxidizing Atmospheres at 400–700 °C. *Corros. Sci.* **2000**, *42*, 1093–1122. [CrossRef]
59. Kofstad, P. *High Temperature Corrosion*; Elsevier: London, UK, 1988.
60. Song, B.; Voisey, K.T.; Hussain, T. High Temperature Chlorine-Induced Corrosion of Ni50Cr Coating: HVOLF, HVOGF, Cold Spray and Laser Cladding. *Surf. Coat. Technol.* **2018**, *337*, 357–369. [CrossRef]

Disclaimer/Publisher's Note: The statements, opinions and data contained in all publications are solely those of the individual author(s) and contributor(s) and not of MDPI and/or the editor(s). MDPI and/or the editor(s) disclaim responsibility for any injury to people or property resulting from any ideas, methods, instructions or products referred to in the content.